ELSEVIER

Journal of Nuclear Materials 248 (1997) 91–100

journal of nuclear materials

Section 5. Tritium interactions with solid breeder surface

Advanced understanding of the tritium recovery process from the ceramic breeder blanket

Carl E. Johnson *, John P. Kopasz, Shiu-Wing Tam

Chemical Technology Division, Argonne National Laboratory, 9700 South Cass Avenue, Argonne, IL 60439-4837, USA

Abstract

The key to successful operation of a tritium breeder blanket is to understand the tritium transport and release characteristics and the role that hydrogen plays in this process. Indications are that grain size (surface-to-volume ratio) largely determine whether tritium release is limited by diffusion or desorption. That is, the larger the grain size the higher the probability that bulk diffusion will determine the release rate. For smaller grain size, the actions taking place on the grain surface become extremely important especially as regards the role that hydrogen plays in the overall process. Experimental studies have indicated that the presence of 0.1% H_2 in the helium purge gas enhances the release of tritium from the lithium ceramic. The tritium released has been found in the form of both HT and HTO. The ab initio calculations on the dissociative hydrogen chemisorption on lithium oxide surfaces provide one component of the quantitative basis for an understanding of the role of hydrogen in affecting the release of tritium from lithium ceramic breeders. These calculations suggest heterolytic adsorption of hydrogen onto the ceramic surface. © 1997 Elsevier Science B.V.

1. Introduction

For development of fusion energy as a power source, it is imperative that sufficient supplies of tritium fuel be available to sustain the D/T fusion reaction. To secure an adequate tritium supply, current fusion reactor designs contain a breeder blanket for production of tritium. The blanket in the fusion reactor serves two primary functions: breeding tritium and converting the released energy into sensible heat. Lithium ceramics have been investigated and found to be attractive materials for use as tritium breeder materials. In numerous in-pile experiments on tritium release [1–5], it has been shown that hydrogen enhances tritium release from lithium ceramics. Tritium release is particularly facile when an argon or helium purge gas containing hydrogen, typically at levels of about 0.1%, is used. However, the addition of hydrogen to the purge gas imposes a penalty when it comes to recovery of the tritium produced in the blanket. In particular, a large amount of hydrogen in the purge gas will necessitate a larger multiple-stage tritium purification unit which could translate into higher costs. Optimizing tritium release while minimizing the amount of hydrogen necessary in the purge gas requires a deeper understanding of the tritium release process, especially the interactions of hydrogen with the surface of the lithium ceramic.

Tritium transport and release from a lithium ceramic breeder material is a complex process involving diffusion in the grain, trapping, grain boundary diffusion, surface reactions, desorption and molecular diffusion in the gas phase. In this paper we review recent studies that address the importance of surface reactions and desorption in determining tritium release characteristics and the rate limiting mechanisms. Also recent models used to describe the interaction of hydrogen with the ceramic breeder surface and its role in the tritium release process is discussed.

2. Tritium transport and release

The early irradiation's of lithium ceramics focused primarily on tritium diffusion as the dominant mechanism for tritium release [1–5]. Many studies focused on the tritium transport behavior in lithium aluminate [6–11], one

* Corresponding author. Tel.: +1-630 252 7533; fax: +1-630 252 4176; e-mail: johnsonce@cmt.anl.gov.

PII S0022-3115(97)00203-1

of several candidate ceramic breeder materials. Many assumed that diffusion was the rate limiting mechanism for tritium transport and release from $LiAlO_2$ and the rate constant for tritium diffusion in $LiAlO_2$ was calculated from release experiments. Tritium diffusivity values ranging over six orders of magnitude were reported. In addition, the question as to whether diffusion or desorption was the rate-limiting mechanism was strongly debated [12–16]. In the sections that follow the various steps in the tritium release process are described. In Section 2.1 attention is focused on bulk transport processes that enables tritium to reach the grain surface. In Section 2.2 the processes taking place on the ceramic surface during tritium release are examined with attention being given to the role that hydrogen and the surface play in the tritium release process. Section 2.3 describes the use of a sophisticated computer code to examine the interaction of hydrogen with the lithium ceramic surface for further insight into the details of the tritium release mechanism.

2.1. Tritium transport in the bulk

The liberation of tritium from a neutron irradiated lithium ceramic is composed of at least two consecutive processes, the diffusive motion of the tritium atom within the solid and its subsequent release from the surface of the ceramic. It is important to distinguish the rate controlling step contributing to tritium release. The rate controlling step has been observed to change from surface phenomena to diffusion as the grain size of the specimen increases and as temperature increases. In order to address tritium release issues, one needs a firmer understanding of the mechanism through which hydrogen enhances tritium release.

One reason for the wide range in reported values for tritium diffusion is that measurements were performed under conditions where desorption from the ceramic surface was actually the rate-controlling release mechanism. Generally, the method for determining the diffusion and desorption rate constants has been to observe tritium release from the ceramic and analyze the time dependence of the release process. The data are analyzed using a diffusion, desorption, or a mixed diffusion–desorption model. Complementary measurements that would indicate whether release is in the diffusion- or desorption-controlled regime are usually not made. Recently, Bertone [17], Quanci [18] and Verrall [19] have employed mathematical tests based on the initial slopes of plots of the natural log of the fraction released versus time to determine whether release falls into the diffusion or desorption regime.

Bertone [17] may have been the first to address the boundary conditions that define whether bulk diffusion or surface desorption is the rate limiting step in tritium release. This study indicated that tritium release is controlled by: (1) diffusion of tritium through the crystal when the dimensionless group $ak/D > 10$, (2) desorption of tritiated water from the crystal surface when $ak/D < 1$ and (3) a combination of these processes when $1 < ak/D < 10$, where a is a characteristic crystal size, k is the governing desorption rate constant and D is the governing diffusion coefficient. As both the diffusion coefficient and the desorption rate constant are temperature dependent, this approach indicates that the form of the rate controlling mechanism depends primarily on crystal size and release temperature (see Fig. 1). Bertone [17] suggested that this approach has wide applicability for mixes of sizes and shapes of the ceramic particles and for various conditions.

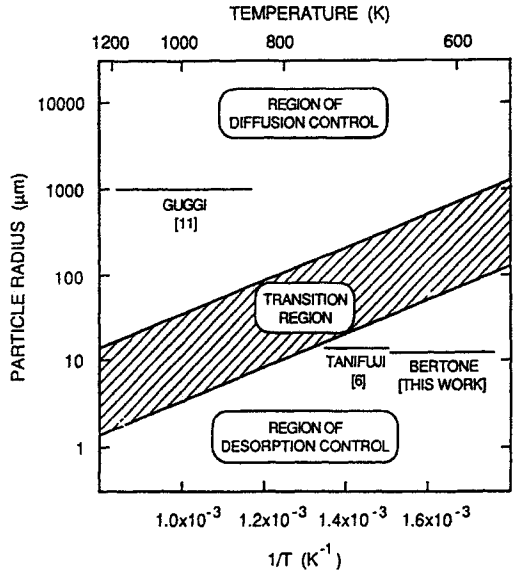

Fig. 1. Summary of tritium release model [17]. The figure outlines tritium release as a function of grain size and temperature.

Following the work of Bertone [17], Quanci [18] conducted a detailed experimental program on single crystal Li_2O to test the postulates. From the solution to Fick's law one can show that the fraction of tritium released as a function of time is

$$f = 1 - 6/\pi^2 \Sigma 1/n^2 \exp(-n^2\pi^2 Dt/a^2), \quad (1)$$

where f is the fraction released, D is the diffusion coefficient, t is the temperature and a is the grain diameter. To distinguish diffusion controlled release one must probe the behavior of f at small times using the following test:

$$\lim(t \Rightarrow 0) \mathrm{d}\ln(f)/\mathrm{d}\ln(t) = 1/2. \quad (2)$$

If tritium release is governed by the release of tritium from the crystal surface, the internal migration of tritium occurs at a much faster rate than desorption from the surface. As a result the governing release equation can be derived by simply equating the decrease in the crystal's internal tritium concentration with the flux of tritiated species emanating from the crystal surface and

$$4/3\pi a^3 \mathrm{d}C(t)/\mathrm{d}t = -4\pi a^2 kC(t), \quad (3)$$

where C is the concentration and k is a first order rate constant. By integrating Eq. (3) over time, one can show that the fraction of tritium released (f) is

$$f = 1 - \exp(-3kt/a). \quad (4)$$

Again, probing the early stages of release and for small values of time:

$$\lim(t \Rightarrow 0)\mathrm{d}\ln(f)/\mathrm{d}\ln(t) = 1. \quad (5)$$

Using single crystal lithium oxide of 10, 100 and 1000 μm in diameter, Quanci [18] collected experimental data that confirmed the appropriateness of the Bertone approach.

Frequently, the initial release behavior does not follow the prescribed mathematics due to time delays in the recorded tritium release or because of the vagaries in the mathematics and the experimental apparatus. Verrall [19] established a more rigorous methodology for the Bertone approach when he identified the need to initiate analysis at a particular time in the tritium release process. In practice, the release rate of tritium will never follow the diffusion-controlled relation at small times, even when the release of tritium is controlled by diffusion, because the formula diverges (goes to infinity) at $t = 0$, showing that the formula can not be meaningful at $t = 0$. Ionization chambers and proportional counters have a relatively large internal volume that contains the tritium that is being measured. As the tritium enters the chamber, the tritium concentration in the chamber increases from zero to a finite maximum and then decreases. Under these conditions, the measured release rate did not follow the relationship $\mathrm{d}\ln(f)/\mathrm{d}\ln(t) = 1/2$, especially at small times. Surprisingly, no matter what the shape of the release curve and no matter what point along the curve is selected as $t = 0$, the relationship $\mathrm{d}\ln(f)/\mathrm{d}\ln(t)$ was found to be equal to 1. Although this limit is 1 for all tritium release curves, diffusion and desorption control can still be distinguished by examining $\mathrm{d}\ln(f)/\mathrm{d}\ln(t)$, not in the limit as t goes to zero, but for longer times, i.e., many times the detector time constant. Thus, the shape of the logarithmic derivative over long times can be used to distinguish between diffusion and desorption controlled release.

Another factor that was thought to contribute to the spread in the reported diffusion coefficients was the presence of impurities in the lithium ceramic. Impurities can alter the diffusivity by creating vacancies, interstitials, or other defects. In lithium aluminate, it has been postulated that tritium diffusion occurs via a lithium-vacancy tritium complex [20]. If this is the case, then impurities that affect the number of lithium vacancies should also affect the tritium diffusivity. The sensitivity of the tritium diffusivity to these impurities depends on the number of lithium vacancies caused by the impurity relative to those defects present in the pure material.

Experimentally, it may be possible to address these difficulties simply by examining the tritium distribution within the ceramic. In the bulk, contributions from desorption are expected to be small and should be limited to the near-surface region. Therefore, the concentration gradient in the interior should be less sensitive to the desorption rate constant, making it possible to obtain good values for the diffusion coefficient, even in the mixed diffusion–desorption regime. Isothermal anneal tests were performed [21] on single-crystal samples (approximately 1.5 mm diameter) to determine the diffusivity of tritium in lithium aluminate. Large single crystals were used to minimize contributions from desorption. Diffusion kinetics become more dominant as the crystal radius increases due to the decreasing surface area-to-volume ratio. However, the release may still be in the mixed diffusion–desorption regime, which would make obtaining the rate constants from the time dependence of the tritium release difficult. Therefore, the experimental approach was to section the sample after each anneal and determine the diffusivity from the tritium concentration profile within the sample. Further, to understand the effects of impurities on the tritium transport, the tritium profiles in pure and Mg-doped (0.3%) $LiAlO_2$ have been studied.

Tritium release from single-crystal lithium aluminate [22] was modeled by assuming diffusion in the bulk with desorption occurring at the surface. The differential equations governing the tritium transport are

$$\partial C/\partial t = D\left(\partial^2 C/\partial r^2 + 2/r\partial C/\partial r\right) \quad \text{for } 0 < r < a \quad (6)$$

and

$$\partial C/\partial r + KC/D = 0 \quad \text{for } r = a. \quad (7)$$

The solution to Eqs. (6) and (7) for the case of a constant initial concentration C_i is given by Carslaw and Jaeger [23]:

$$C = 2hC_i/rG\exp(-D\alpha_n t)\left[a^2\alpha_n + (ah-1)^2\right]/\alpha_n \times \left[a^2\alpha_n + ah(ah-1)\right]\sin(a\alpha_n)\sin(r\alpha_n), \quad (8)$$

where C is the concentration at position r, k is the desorption rate constant, D is the diffusivity, $h = k/D$, C_i is the initial concentration, a is the crystal radius, r is the radial position, t is the time, and α_n represents the roots of $a_n^{\alpha}\cot(a_n^{\alpha}) = 1 - ah$.

One can determine the diffusivity and desorption rate constant given the tritium concentration at the surface, the tritium concentration at the center, and the initial tritium concentration; a better method might be to fit the total observed tritium profile to Eq. (8). This approach would minimize errors due to measuring the very small crystals left at the end of the dissolution step. Diffusivities were obtained from the initial concentration (determined from the sum of the tritium collected in ethylene glycol traps during the anneal and the tritium remaining in the sample determined by sectioning) and a minimization routine that fit the concentration data to Eq. (8) (see Fig. 2).

Tritium diffusivity was observed to follow a simple Arrhenius- type temperature dependence, with the diffusivity determined for the doped and undoped materials being the same within experimental error. This suggests that impurities which create lithium vacancies have little or no effect on tritium diffusion in lithium aluminate over the temperature range investigated.

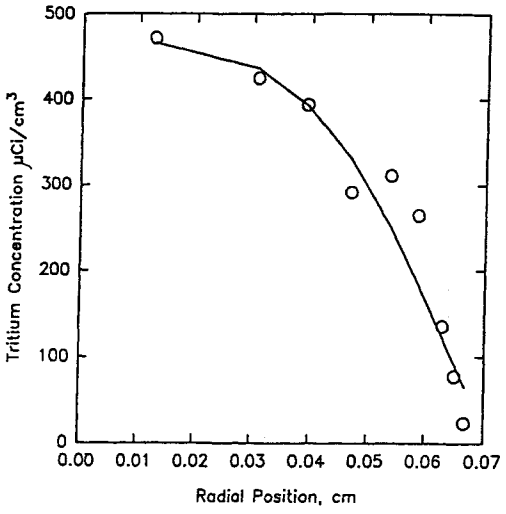

Fig. 2. Observed and calculated tritium profile for pure $LiAlO_2$ annealed at 1056 K for 4500 s ($D = 3.24 \times 10^{-12}$ m^2/s, $K = 9.0 \times 10^{-8}$ m/s).

Tritium desorption rate constants determined by the sectioning method exhibited some scatter. The scatter may be due to experimental difficulties in determining the concentration at the surface, or to a more complex surface desorption processes in which different mechanisms function at different temperatures. The latter explanation would be in agreement with previous temperature-programmed desorption (TPD) [16] experiments which indicate several desorption mechanisms. Using the values determined for D and k from the large single crystals, desorption will be rate controlling when the ratio ak/D is less than or equal to 1. For grain radii less than 100 μm, the tritium transport will be in the desorption-controlled regime. Thus, for in-pile tests where $a < 100$ μm these results suggest that tritium release should be desorption controlled.

2.2. *Tritium desorption from the ceramic surface*

While desorption has been determined to be the rate-limiting step in tritium release [24–26], the details of the release process are still receiving attention. Early on, tritium desorption was treated as occurring from one site with one desorption activation energy. However, in recent experimental studies [27–29], the rate of evolution of $H_2O(g)$ was observed to go through several maxima which was interpreted as indicating that evolution proceeded from several types of desorption sites, each with its corresponding activation energy. Isotherms and isobars derived from the adsorption data revealed two processes with different activation energies for adsorption. Also, the heats of adsorption were found to depend upon the degree of surface coverage.

In developing theoretical models of tritium release from ceramic breeder materials, the activation energy of desorption is an important variable. The activation energy for desorption is equal to the sum of the heat of adsorption and the activation energy of adsorption. Usually, the activation energy of adsorption is small so that the activation energy of desorption is approximated by the heat of adsorption. It follows that the activation energy of desorption is a function of surface coverage as is the heat of adsorption. The observed range of values for the heat of adsorption indicates a range of activation energies for desorption. The physical basis for such a range is the existence of multiple types of sites for adsorption and, hence, multiple types of sites from which desorption occurs. For example, a theoretical analysis of the types of OH^- sites possible on the surface of alumina, characterized in terms of the number of O^{2-} nearest neighbors, showed five different types of sites to be present.

The complexity of the $H_2O(g)$ adsorption/desorption process for lithium aluminate has recently been examined [30]. Reactivity differences in adsorption sites could be that one kind of adsorption site involves lithium ions and adjacent oxides and another kind of site involves aluminum ions and adjacent oxides. Further evidence from a number of studies on candidate ceramic breeder materials indicate multiple types of sites, with their associated activation energies for desorption, are involved in the desorption of $H_2O(g)$, $HTO(g)$, or $T_2(g)$ from the ceramic breeder surface [31]. The degree of surface coverage by adsorption of $H_2O(g)$ or $H_2(g)$ and diffusion of tritium to the grain surface will determine which type of site is dominant in the release process and what the desorption activation energy will be at that time. Related studies have shown that multiple desorption processes are involved in the evolution of H_2O (T_2O) from the lithium ceramics [31]. These processes differ in several respects: (1) they can involve chemisorption or physisorption, (2) there can be different degrees of surface coverage by OH^- groups and (3) differing types of surface sites from which desorption occurs. The distinction in sites may involve defects, impurities and differences in ions on different crystallographic planes exposed to the gas phase.

A study of hydrogen adsorption/desorption from lithium oxide using a combination of temperature programmed desorption (TPD) and diffuse reflectance infrared Fourier transform spectroscopy (DRIFTS) measurements was carried out to gain information about the species present on the surface of the lithium ceramic and their relationship to tritium desorption. From the shape and position of the desorption peak in the TPD spectra one can obtain information about the energetics of the desorption process [32]. However, as TPD provides no information on the identity or form of the species desorbing from the surface, DRIFTS fills this gap and provides the information on the identity of surface species.

The hydroxyl region of the DRIFTS spectra for lithium oxide powder was examined after exposure to a purge gas of $Ar + 0.1\%D_2$ at 365°C. Several different absorption

peaks were observed for OH and OD. Under different conditions, other peaks appear more prevalent. Deconvolution of these curves indicates four different OH absorption peaks at: 3657, 3604, 3480 and 3400 cm^{-1}. Upon exposure to D_2, corresponding OD peaks were observed at 2695, 2659 and 2560 cm^{-1}. (The OD peak corresponding to the OH peak at 3400 cm^{-1} was not observed, probably due to the very low intensity of this band under the conditions investigated.) These results suggest that there are four different OH species on the surface. We propose that these are OH species with coordination numbers of 2, 4, 6 and 8, respectively. The strength of the OH bond and, therefore, the OH vibration frequency, will depend on the electron density on the oxygen. As the electron density on the oxygen is reduced by coordination to Li atoms in the lattice, the O–H bond strength should decrease, decreasing the frequency of the absorption. This is similar to the effect seen for infrared absorption of terminal versus bridging carbonyl groups [33].

Under certain conditions, infrared absorption peaks were observed in the region where a Li–H stretch is expected ($\sim$ 1280 cm^{-1}). At temperatures above 380°C and with a purge gas of Ar + 0.1% hydrogen, absorption peaks occur over the range 1245 to 1212 cm^{-1}. When the purge gas is changed to pure argon, these peaks disappear suggesting that these absorptions may be due to the presence of a Li–H species on the surface. The fact that the infrared peaks at 1245 to 1212 cm^{-1} are shifted to slightly lower frequencies than that observed for bulk lithium hydride (1280 cm^{-1}), may be due to a bridging hydride. Confirmation that these peaks are due to hydride formation by isotopic substitution with deuterium has not been possible since deuterium shifts the peaks to a position beyond the absorption edge. The presence of a LiH species on the surface suggests that hydrogen is heterolytically adsorbed on the surface to form $H^+(OH^-)$ and $H^-(LiH)$. Quantum mechanical calculations indicate that this type of heterolytic adsorption could be expected on some lithium oxide surfaces [34].

The combination of the TPD curve and the DRIFTS results suggests that the TPD peak observed at about 390°C (663 K) is due mainly to removal of the OH species from the surface. The observation of this species at the surface and the observed change in the concentration of this species with time indicate that the rate-controlling mechanism for the disappearance of this peak is not bulk diffusion. If bulk diffusion were the rate controlling process, one would expect the surface concentration to be near zero and no appreciable change in the surface concentration of this species would be observed during the TPD peak.

2.3. Quantum mechanical description for tritium release

A better grasp of the role of hydrogen in the tritium release process may be gained through an understanding of the mechanism by which hydrogen enhances tritium release. A mathematical approach employing computer simulation technology has been used to model the processes involved in the adsorption of hydrogen onto the lithium oxide surface. The methodology is guided by the understanding obtained from ab initio calculations of hydrogen chemisorption on Li_2O surfaces. The constraints placed on the mechanistic processes by stoichiometry requirements were examined and leads to consideration of both surface steps and point defects.

The technique that has been employed is the self-consistent-field Hartree–Fock method with linear-combination of atomic orbitals (LCAO) modified to a crystalline environment. The *ab initio* method, contains no ad hoc adjustable parameters and uses crystal orbitals (COs) instead of molecular orbitals (MOs) [34–36]. These COs are defined (similar to the molecular orbital approach) as a linear-combination of atomic orbitals but with the periodic environment of the crystal built-in. This approach takes the extended nature of the crystalline lattice into account. The CRYSTAL code [37] that we use for such calculations has adopted this CO approach. However, for some low symmetry configurations, such as kinks and ledges on surface step structures, the CRYSTAL approach may not be practical. In such situations a finite cluster approach, based on the GAUSSIAN90 code [38], was found to be more suited to simulate the low symmetry configurations. Both codes have been utilized in a complementary manner. The main emphasis of the study was to investigate the possibility for dissociative hydrogen chemisorption on the unrelaxed terrace sites of Li_2O surfaces with the CRYSTAL code being the principle tool used [34].

A slab model was also used when the semi-infinite lithium oxide crystal was simulated by a finite number of atomic layers parallel to the crystal surface. Hydrogen adsorption onto the (110) and (111) terraces of lithium oxide, and the step structures on the (110) terrace has been investigated. Surface reactivity has been analyzed using an analysis of the change in the local density of states (DOS) as a function of the change in the local environment.

One of the keys to a successful ab initio calculation, is obtaining a good basis set to represent the electronic structure of the species. In the case of lithium oxide, its bonding characteristic is strongly ionic. In free space, the O^{2-} is an unstable ion; however, in crystalline Li_2O, the anion is stabilized by the surrounding Li^+ ion environment. In this situation, the two extra electrons on the oxygen ion would induce a relaxation of the valence electrons. This particular consideration for O^{2-} is necessary for any oxide in which the bonding is reasonably ionic. This effect is taken into account in an optimized basis set designed for the oxygen ion in an Li_2O environment. Recent calculations on bulk crystalline Li_2O done by Dovesi et al., [39] have indicated that the optimized basis set, [14s/6p] and [7s/1p] for oxygen and lithium, respectively, yields lattice constants, elastic constants, and

Table 1
Comparison of the energy and geometrical parameters from Hartree–Fock calculations with that from experiment

	Dovesi [39]	Experiment
Total energy (eV)	−2447.920	–
HF cohesive energy (eV)	7.864	11.755 [a]
Lattice parameter (Å)	4.57	4.57 [42]
Bulk modulus (dyn cm^{-2})	0.93×10^{12}	0.85×10^{12} [42]

[a] Obtained with an atomic reference from thermochemical data [44].

central zone phonon frequencies in good agreement with experimental values. Table 1 lists the results of the calculations and the corresponding experimental data. We have adopted this crystalline basis set [39] for our calculations involving lithium oxide. For hydrogen, the basis set [7s/1p] obtained by Dovesi [40] was used, wherein the calculated equilibrium Hartree–Fock bond length of H_2 of 0.738 Å is in good agreement with its experimental value of 0.742 Å [41].

3. Results and discussion

The geometrical and electronic structures of the bulk Li_2O, the stability of the Li_2O surfaces and dissociative hydrogen chemisorption on the Li_2O surfaces are discussed in Sections 3.1, 3.2, 3.3 and 3.4. The CRYSTAL code was used unless stated otherwise.

3.1. Crystalline and electronic structure of Li_2O

A number of experiments [41–43] have investigated the bulk properties of crystalline Li_2O, which has an anti-fluorite structure with the space group $Fm3m$. The experimental lattice constant a_0 at $T = 0$ K is 4.573 Å [42], obtained by extrapolating the a_0 versus T curve measured in the range of 293–1300 K. For the lattice constant of 4.573 Å, the nearest Li–Li, O–O and Li–O distances are 2.286, 3.224 and 1.980 Å, respectively.

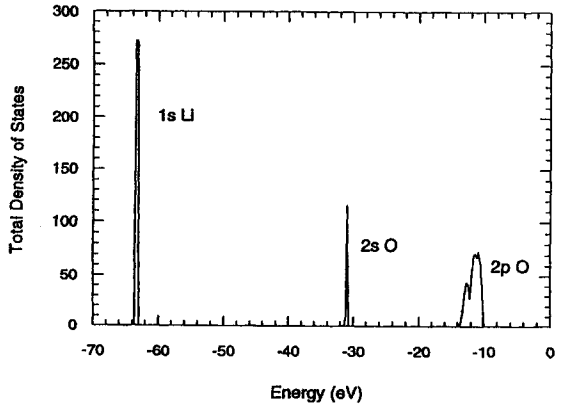

Fig. 3. The Hartree–Fock total density of states of crystalline Li_2O.

The calculated density of states (DOS) for the valence bands of bulk Li_2O are shown in Fig. 3. Fig. 3 identifies the order of the occupied bands of lithium and oxygen according to their energies. It also describes the number of states within an interval of energies between E and $E + dE$. The deepest band, not shown in Fig. 3, occurs at −555.910 eV and is the 1s core orbital from oxygen (O 1s). This band is followed by the two bands of the 1s orbital from lithium (Li 1s), in the interval of −63.451 to −63.105 eV. The 2s orbital of oxygen (O 2s) appears between −31.231 to −30.810 eV and the highest bands located between −13.554 to −10.025 eV are the p orbitals of oxygen (O 2p).

Our ab initio calculation of crystalline Li_2O indicates that it is a strongly ionic material for the following reasons. First, there is little overlap of the ionic charge distribution between the nearest neighboring Li–O bonds, as indicated by the small and negative (−0.01) bond population. This shows the limited presence of covalence. Secondly, as a consequence, the crystalline Li_2O energy bands are well separated and the lithium band does not contribute to the uppermost valence band of oxygen (Fig. 3, O 2p). Finally, from a Mulliken analysis of the charge distribution, the net charge of oxygen is −1.94 eV, very close to the value of −2 eV expected from ideal ionic bonding.

3.2. Stability of unrelaxed Li_2O crystal surfaces

A study of the Li_2O surface was carried out with the slab model. In this model, the semi-infinite Li_2O crystal was simulated by a finite number of atomic layers parallel to the exposed surface, reproducing the crystal geometry. Lithium oxide crystal has three surfaces, namely, (100), (110) and (111). The (100) surface consists of alternating lithium layers and oxygen layers. The distance between the two layers is 1.143 Å. Each layer of the (110) surface is neutral and has both lithium and oxygen on the same plane. The layer separation is 1.617 Å. The (111) surfaces, for the smallest neutral unit, have two lithium layers and one oxygen layer and the oxygen layer is located between two lithium layers. The distance between the lithium and the oxygen layers is 0.660 Å and the distance between the two adjacent lithium layers is 1.320 Å. The stacking of the layers for these different surfaces are shown in Fig. 4.

The charged layers were classified into three classes depending upon the stacking sequences of the charged layers in the bulk of the crystal[45]. The stacks of the (100) planes are charged and have a dipole moment (μ) perpendicular to the planes (Fig. 4a). Addition of an extra neutral unit of two planes to the (100) surface creates a dipole–dipole interaction which will affect the energy of ions within

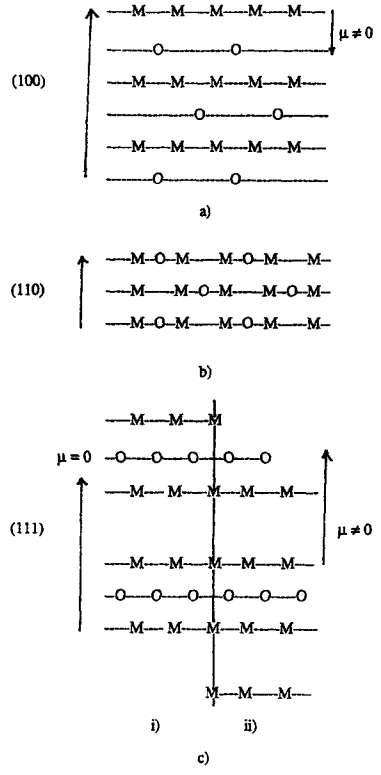

Fig. 4. Stacking sequence of (100), (110), and (111) planes. The non-zero dipole moment (μ) occurs on the (100) and (111) planes, with the anion termination. M denotes Li^+ and O is O^{-2}.

the crystal. The potential, therefore, never settles to its normal bulk value and the surface energy does not converge. Thus, the (100) surface is energetically unstable and, therefore, will not be considered further. Unlike the (100) planes, the (110) layers are built up from a stack of neutral layers (Fig. 4b). Both lithium and oxygen ions are present on each layer in a ratio such that the total charge is zero. The (110) surface is energetically stable since no dipole moment is created by the layer. Addition of (110) layers on the surface will have no electrostatic effect on an ion in the bulk. The (111) planes exhibit two different stackings. For one of these, the surface which terminates with the cation layer (Fig. 4c(i)) has no net dipole moment and is stable. The other, which starts with the anion layer (Fig. 4c(ii)), has a non-zero moment that causes the surface to be unstable. To our knowledge no experimental study has been done on the ordering and faceting properties of Li_2O surfaces.

The surface energy (SE) of (110) and (111) surfaces can be calculated from the following equation [46]: $SE = (nE^b - E^n)/2$ where the denominator 2 is included because the surface energy is calculated with respect to one surface only; n denotes the number of layers, in this case $n = 1, 2, 3, \ldots$ for (110) and $n = 3, 6, 9, \ldots$ for (111); E^b is the total energy (per Li_2O) of the bulk and E^n represents the total energy (per nLi_2O) of the n-layer slab. The surface energy of the stable (110) and (111) surfaces converges as the number of layers increase. The surface energy of (111) converges to 0.679 J m^{-2} while the (110) converges to 1.443 J m^{-2}. A significant change in the surface energy, about 0.239 J m^{-2}, occurs from the one- to two-layer (110) slab as a result of the uncoordinated ions on the single layer. The surface energies with the extended basis set for (111) and (110) calculated by Dovesi et al. [39] are about 15 and 11%, respectively, lower than those calculated by Lichanot et al. [47]. In our work, the surface energy is 0.764 J m^{-2} lower for (111) than (110). This reflects the fact that the (111) surface is the natural cleavage plane in the anti-fluorite structure. Although the (111) surface is energetically more favorable, in reality, one expects that a faceted Li_2O crystal would have both (110) and (111) surfaces present on a typical ceramic surface.

An electronic charge density contour calculation of the three-layer (110) slab shows that a lack of covalence occurs with a clear charge separation between the nearest Li–O neighbors. A similar ionic characteristic was observed for the (111) surface.

3.3. Dissociative hydrogen chemisorption on lithium oxide terraces

In the heterolytic environment around the Li–O sites and for 100% hydrogen coverage, exothermic, dissociative chemisorption of hydrogen occurs on a one-layer (110) slab. The chemisorption reaction produces OH^- with a covalent type of bonding and $Li^+H^-Li^+$ with an ionic type of bonding, where the H^- forms a bridge bond between two lithium sites. However, the calculations for the (110) terraces for an n-layer slab (where $n = 2$ and 3), indicate an endothermic reaction. Therefore, the calculated results suggest that the one-layer terrace is very reactive as compared to a two- or three-layer terrace. For the one-layer case, the local coordination of oxygen and lithium sites is fourfold and twofold respectively, whereas that for multi-layer case is sixfold and threefold, respectively. It would appear that the higher reactivity of the one-layer case is directly related to the lower coordination of the lithium and oxygen sites. Furthermore, the density of states suggests that the reactivity is mainly determined by the characteristics of the O site on the surface. In the one-layer terrace, the top of the valence band is due to the O 2p band; the O $2p_z$ band which is perpendicular to the surface lies at the uppermost energy levels thereby interacting strongly with the H_2 as it approaches the surface while the O $2p_x$ and O $2p_y$ bands lie parallel to the surface and do not contribute to the interaction. However, the addition of layers in a multi-layer terrace stabilizes the O $2p_z$ band to a lower energy level thereby reducing the reactivity of the surface. It should be noted here, that lithium plays a complementary but necessary role to the oxygen in contributing to the reactivity of the surface.

On the (111) surface, the hydrogen chemisorption is endothermic. Due to screening by the two lithium layers, the oxygen sites can not interact directly with the hydrogen. No chemisorption occurs at the homolytic sites, such as, O–O or Li–Li on the (111) surface.

3.4. Dissociative hydrogen adsorption on lithium oxide step structures

In the case of the one-layer (110) terrace, there is indication of dissociative hydrogen adsorption due to the low-coordination of oxygen. Although the one-layer (110) terrace does not realistically represent a solid surface, the simulation results do suggest that the local coordination plays an important role in determining the surface reactivity. Since low-coordination sites on the surface can be found in the presence of defects, hydrogen adsorption on the lithium oxide surface containing step structures was examined.

Two kinds of steps on the (110) surface were examined, type I, a step with infinite ledges along the y-axis and it has a finite step-width along the x-axis, and type II, a step with infinite ledges along the x-axis and a finite width along y-axis. The characteristics of the type I step structure are as follows. The oxygen and lithium sites have the same local coordination as they have in the three-layer terrace namely, sixfold and threefold, respectively. Density of states (DOS) calculations show that the energy levels of the O $2p_z$ band does not constitute the uppermost level. Consequently, the O $2p_z$ band does not interact with hydrogen exothermally for the type I structure. The type II step structure has two different locations for oxygen and lithium sites. For sites along the ledges, lithium and oxygen have lower coordination than those sites located in the terrace region. The oxygen site located along the ledge is therefore very reactive due to its fourfold coordination which lifts the O $2p_z$ band to the uppermost energy level in the valence band. The chemisorption state of a reaction between hydrogen and the type II step structure is very similar to the case of one-layer terrace.

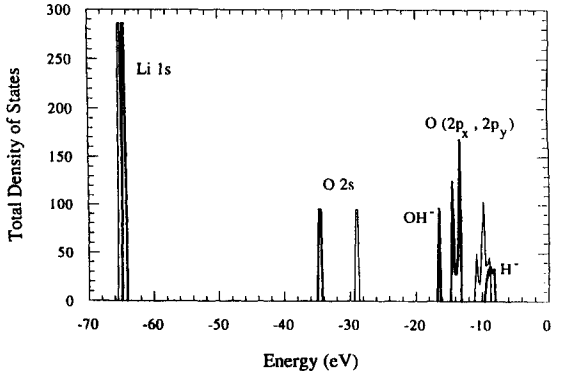

Fig. 5. Density of states for a one layer (110) slab. The fine lines represent the DOS before chemisorption. The thick lines represent the DOS where dissociative hydrogen is chemisorbed.

Fig. 5 shows the local DOS for dissociative hydrogen chemisorption where one of the hydrogen forms OH^- with an oxygen at the oxygen ledge and the other hydrogen makes a bridge bond with the two nearest lithium's forming $Li^+H^-Li^+$. In the presence of the H^+, the O 2p is split into O ($2p_x$, $2p_y$) and O $2p_z$ which is stabilized to a lower energy level. The O $2p_z$ is not only stabilized but also interacts covalently with H^+ forming OH^-. In the figure, we also see the 1s band representing the H^- which interacts ionically with the two adjacent lithium's. Note, for a step structure that has a lower local coordination, such as step II, the step–step interaction affects the surface reactivity. Based on the energetic and DOS analysis, it shows that if we separate the steps further apart from each other, the surface reactivity increases (indicated by the shift of the O 2p band to a higher energy level) and, finally, it is constant at the point where there is no step–step interaction.

4. Conclusions

The key to successful operation of a tritium breeder blanket is to understand the tritium transport and release characteristics and the role that hydrogen plays in this process. Indications are that grain size (surface-to-volume ratio) largely determine whether tritium release is limited by diffusion or desorption. That is, the larger the grain size the higher the probability that bulk diffusion will determine the release rate. For smaller grain size the actions taking place on the grain surface become extremely important especially as regards the role that hydrogen plays in the overall process. Experimental studies have indicated that the presence of 0.1% H_2 in the helium purge gas enhances the release of tritium from the lithium ceramic. The tritium released has been found in the form of both HT and HTO. The ab initio calculations on the dissociative hydrogen chemisorption on lithium oxide surfaces provide one component of the quantitative basis for an understanding of the role of hydrogen in affecting the release of tritium from lithium ceramic breeders. These calculations suggest heterolytic adsorption of hydrogen onto the ceramic surface.

Bombardment of lithium ions by fast neutrons creates tritium in the form of T^+. In this situation, there are several ways in which tritium could escape from the surface. Under normal conditions, a chemical species will be released from a solid surface in a molecular form, such as T_2, T_2O, etc. At steady state and in the presence of irradiation with no hydrogen in the helium purge gas, the concentration of T^+ inside the solid is of the order of a few tens of ppm [2]. If the released form of tritium is in the form of T_2 or T_2O, the rate of release is proportional to the *square* of the tritium concentration in the lithium-based solid breeder material. The probability of forming T_2 or T_2O is very small and release is slow. The slow tritium release in the absence of hydrogen in the purge gas, is

limited by the difficulty of forming molecular species that require two tritium atoms which has been observed in both in-reactor tests as well as laboratory experiments.

However, the presence of hydrogen in the purge gas stream (e.g., as an additive $\sim 0.1\%$–1% H_2), provides a very different environment. The hydrogen is chemisorbed onto the lithium ceramic surfaces forming OH^- and $Li^+H^-Li^+$, with which there are two possible reactions with the T^+:

$$Li^+H^-Li^+ + T^+ = 2Li^+ \text{ (solid)} + HT \quad (9)$$

or

$$OH^- + T^+ = HTO + O^{2-} \text{ (vacancy)}. \quad (10)$$

In both tritium release processes, the rate scales as the product of the surface coverage of the chemisorbed hydrogen species and the tritium concentration. However, the rate is not well characterized so there remains some doubt as to the details of the surface interactions in the tritium release process. The hydrogen coverage is usually much larger than the tritium concentration. Therefore, the tritium release rate is proportional to the first power in the tritium concentration and not to its square as is the case in the absence of hydrogen. This is the basic reason that the addition of hydrogen to the purge gas lead to an enhancement of the tritium release rate.

Relying on only the 'intrinsic' impurity hydrogen concentration which is present to the level of a few ppm in nominally 'pure ' helium is unlikely to be effective, since in that case the chemisorbed hydrogen surface coverage would then be correspondingly very low. The rates of HT and HTO formation would be no better or even lower than that of T_2 and T_2O. One needs to add hydrogen to a level substantially above the 'normal' impurity level in order for it to be effective in enhancing tritium release. Present understanding would also suggest that the tritium release rate cannot be enhanced arbitrarily by simply increasing the hydrogen partial pressure in the helium purge stream. In other words there is a saturation effect. This can be understood from the fact that our simulations have indicated that a majority of the surface sites (i.e., the terrace sites) are *not* available for hydrogen chemisorption. Only a minority amount of sites (such as step ledges and point defects) are favorable. Once those sites are all occupied further increases of the hydrogen partial pressure would not be useful (e.g., $> 0.5\%$).

References

[1] R.G. Clemmer, P.A. Finn, B. Misra, M.C. Billone, A.K. Fischer, S.W. Tam, C.E. Johnson, A.E. Scandora, J. Nucl. Mater. 133&134 (1985) 171.

[2] O.D. Slagle, G.W. Hollenberg, Beatrix-II, Phase I: Data Summary, Pacific Northwest Laboratory Report PNL-10279, 1995.

[3] K. Okuno, H. Kudo, J. Nucl. Mater. 138 (1984) 210.

[4] E. Roth, J.J. Abassin, F. Botter, M. Briec, P. Chenebault, M. Masson, B. Rasneur, N. Roux, J. Nucl. Mater. 133&134 (1985) 238.

[5] T. Kurasawa, H. Watanabe, G.W. Hollenberg, Y. Ishii, A. Nishimura, H. Yoshida, Y. Naruse, M. Aizawa, H. Ohno, S. Konishi, J. Nucl. Mater. 141–143 (1986) 265.

[6] D. Bruning, D. Guggi, H.R. Ihle, Fusion Technol. 1 (1982) 543.

[7] R.G. Clemmer, P.A. Finn, R.F. Malecha, B. Misra, M.C. Billone, D.L. Bowers, A.K. Fischer, L.R. Greenwood, R.F. Mattas, S.W. Tam, R.B. Poeppel, G.T. Reedy, I.T. Dudley, F.F. Dyer, E.D. Clemmer, J.S. Watson, P.W. Fischer, J.R. Conlin, R.L. Childs, J.L. Scott, R.M. Arons, A.E. Scandora, The TRIO Experiment, Argonne National Laboratory, Report ANL-84-85, 1984.

[8] F. Botter, D. Cherquitte, N. Roux, in: Proceedings of the 14th SOFT (Pergamon, New York, 1986) p. 1537.

[9] K. Okuno, H. Kudo, J. Nucl. Mater. 138 (1986) 357.

[10] S. Tanaka, A. Kawamoto, M. Yamawaki, T. Terai, Y. Takahashi, H. Kawamura, M. Saito, Fusion Eng. Des. 8 (1989) 155.

[11] J.P. Kopasz, C.A. Seils, C.E. Johnson, J. Nucl. Mater. 191–194 (1992) 231.

[12] H. Kudo, K. Okuno, J. Nucl. Mater. 133&134 (1985) 192.

[13] M. Dalle Donne, Fusion Technol. 9 (1986) 503.

[14] H. Kwast, A. Kout, R.P. Muis, M.P. Stijkel, A.J. Flipot, J.D. Elen, Fusion Eng. Des. 8 (1989) 359.

[15] T. Tanifuji, K. Noda, S. Nasu, K. Ushida, J. Nucl. Mater. 95 (1980) 108.

[16] W. Dienst, D. Schild, H. Werle, Kernforschungszentrum Karlsruhe, Report KfK-5109, 1992.

[17] P.C. Bertone, J. Nucl. Mater. 151 (1988) 281.

[18] J.F. Quanci, dissertation, Department of Chemical Engineering, Princeton University (1989).

[19] R. Verrall, in: Proc. Int. Workshop on Ceramic Breeder Blanket Interactions (Argonne National Laboratory, Argonne, IL, 1992) p. 91.

[20] J.P. Kopasz, S.W. Tam, C.E. Johnson, J. Nucl. Mater. 179–181 (1991) 816.

[21] J.P. Kopasz, C.A. Seils, C.E. Johnson, J. Nucl. Mater. 212–215 (1994) 912.

[22] N. Roux, CEA, personal communication (1990).

[23] H.S. Carslaw, J.C. Jaeger, Conduction of Heat in Solids (Clarendon, Oxford, 1959) p. 238.

[24] M. Briec, F. Botter, J. J Abassin, P. Chenabault, M. Masson, B. Rasneur, P. Sciers, H. Werle, E. Roth, J. Nucl. Mater. 141–143 (1986) 357.

[25] P.C. Bertone, J. Nucl. Mater. 151 (1986) 281.

[26] W. Breitung, H. Elbel, J. Lebkucher, G. Schumacher, H. Werle, J. Nucl. Mater. 155–157 (1988) 507.

[27] T. Tanufugi, K. Noda, S. Nasu, K. Uchida, J. Nucl. Mater. 95 (1980) 108.

[28] A. Skokan, H. Wedemeyer, E. Gunther, H. Werle, 15th SOFT, Utrecht, The Netherlands, Sept. 1988.

[29] V. Schauer, G. Schumacher, STNM-7 Chicago, IL, Sept. 1988.

[30] A.K. Fischer, C.E. Johnson, Fusion Technol. 15 (1989) 1212.

[31] J.P. Kopasz, A.K. Fischer, C.E. Johnson, Adv. Ceram. 27 (1990) 317.

[32] J.L. Falconer, J.A. Schwarz, Catal. Rev. Sci. Eng. 25 (2) (1982) 141.

[33] M. Tamiguchi, S. Tanaka, in: Proc. 4th Inte. Workshop on Ceramic Breeder Blanket Interactions, Oct. 9–11, 1995, Kyoto, Japan, p. 298.
[34] A. Sutjianto, S.W. Tam, R. Pandy, L.A. Curtiss, C.E. Johnson, J. Nucl. Mater. 219 (1995) 250.
[35] G. Del Re, J. Ladik, G. Biczo, Phys. Rev. 155 (1967) 997.
[36] L. Gouverneur, G. Leroy, Int. J. Quantum Chem. 1 (1967) 451.
[37] R. Dovesi, C. Roetti, V.R. Saunders, CRYSTAL92 program.
[38] M.J. Frisch, M. Head-Gordon, G.W. Trucks, J.B. Foresman, H.B. Schlegel, K. Ragavachari, M.A. Robb, J.S. Binkley, C. Gonzalez, D.J. Freeze, D.J. Fox, R.A. Whiteside, R. Seeger, C.F. Melius, J. Baker, R.L. Martin, L.R. Kahn, J.J.P. Stewart, S. Topiol, J.A. Pople, Gaussian, Pittsburgh, PA, 1990.
[39] R. Dovesi, C. Roetti, C. Freyria-Fava, M. Prencipe, Chem. Phys. 156 (1991) 11.
[40] R. Dovesi, C. Ermondi, E. Ferrero, C. Pisani, C. Roetti, Phys. Rev. B29 (1984).
[41] T.W.D. Farley, W. Hayes, S. Hull, R. Ward, M.T. Hutchings, M. Alba, Solid State Ionics 28–30 (1988) 189.
[42] S. Hull, T.W.D. Farley, W. Hayes, M.T. Hutchings, J. Nucl. Mater. 160 (1988) 125.
[43] T.W.D. Farley, W. Hayes, S. Hull, M.T. Hutchings, M. Alba, M. Vrtis, Physica B156&157 (1989) 99.
[44] R.C. Weast, ed., The Handbook of Chemistry and Physics, 67th Ed. (CRC, Cleveland, OH, 1986–1987).
[45] P.W. Tasker, Surf. Sci. 78 (1979) 315.
[46] C. Pisani et al., Hartree–Fock Ab Initio Treatment of Crystalline Structure (Springer, Berlin, 1988) p. 136.
[47] A. Lichanot, M. Gelize, C. Larrieu, C. Pisani, J. Phys. Chem. Solids 52 (1991) 1155.